

A Robust Age Indicator for Old Stellar Populations

A. Vazdekis & N. Arimoto

Institute of Astronomy, School of Science, University of Tokyo, Osawa 2-21-1, Mitaka, Tokyo 181-8588,
Japan

(e-mail: vazdekis@mtk.ioa.s.u-tokyo.ac.jp, arimoto@mtk.ioa.s.u-tokyo.ac.jp)

Received _____; accepted _____

arXiv:astro-ph/9906140v1 8 Jun 1999

ABSTRACT

We derive new spectral $H\gamma$ index definitions which are robust age indicators for old and relatively old stellar populations and therefore have great potential for solving the age-metallicity degeneracy of galaxy spectra. To study this feature as a function of age, metallicity and resolution, we have used a new spectral synthesis model which predicts spectral energy distributions of single-age, single-metallicity stellar populations at resolution $\text{FWHM} \sim 1.8\text{\AA}$ (which can be smoothed to different resolutions), allowing direct measurements of the equivalent widths of particular absorption features. We show that $H\gamma$ strong age disentangling power is due to a compensating effect: at specified age, $H\gamma$ strengthens with metallicity due to an adjacent metallic absorption, but on the other hand the adopted pseudocontinua are depressed by the effects of strong neighboring FeI lines on both sides of $H\gamma$. Despite the fact that this effect depends strongly on the adopted resolution and galaxy velocity dispersion σ , we propose a system of indicators which are completely insensitive to metallicity and stable against resolution, allowing the study of galaxies up to $\sigma \sim 300 \text{ km s}^{-1}$.

An extensive analysis of the characteristics of these indices indicates that observational spectra of very high signal-to-noise ratio and relatively high dispersion, are required to gain this unprecedented age discriminating power. Once such spectra are obtained, accurate and reliable estimates for the luminosity-weighted average stellar ages of these galaxies will become possible for the first time, without assessing their metallicities. We measured this index for two globular clusters, a number of low-luminosity elliptical galaxies and a standard S0 galaxy. We find a large spread in the average stellar ages of a sample of low-luminosity ellipticals. In particular, these indices yield 4 Gyr for M 32. This value is in excellent agreement with the age provided by an extraordinary fit to the full spectrum of this galaxy that we achieve in this paper.

Subject headings: galaxies: abundances — galaxies: elliptical and lenticular, cD — galaxies: evolution — galaxies: stellar content — globular clusters: general

1. Introduction

The understanding of the stellar populations of early-type galaxies plays a key role in assessing the origin of these systems. Elliptical galaxies yield robust color-magnitude relations, as shown with high photometric precision by Bower, Lucey & Ellis (1992) for the Virgo and Coma clusters. The origin of this color-magnitude relation is under a strong debate; the relation could either be caused by a variation of the mean stellar metallicity along the relation (e.g., Arimoto & Yoshii 1987; Kodama & Arimoto 1997), or it can be attributed to a variation of the age and metallicity (Ferreiras, Charlot & Silk 1998). This is because the interpretation of the stellar populations from the integrated light of galaxies suffers from the fact that there is an age-metallicity degeneracy, i.e, the two effects cannot be separated simultaneously with current techniques (O’Connell 1986; Worthey 1994; Arimoto 1996).

One expects that, rather than using colors, more accurate spectral information should be able to break this degeneracy. In particular, Balmer lines were thought to be ideal candidates, because younger (i.e. hotter) stars show stronger hydrogen absorption (O’Connell 1976). However, Worthey (1994) showed that use of $H\beta$ at intermediate spectral resolution ($\sigma \sim 200 \text{ kms}^{-1}$) together with a large set of the other Lick metallic absorption lines is not enough to provide the desired age-metallicity discrimination. Therefore more accurate and reliable estimates for the ages of early-type galaxies are crucial in understanding their formation. Worthey & Ottaviani (1997) showed the importance of increasing resolution when working with Balmer lines, and Jones & Worthey (1995) (hereafter JW95) have shown the ability of their $H\gamma_{HR}$ (a redefinition of Rose 1994 $H\gamma$ index) high resolution index to separate the metallicity and age effects.

In this paper we study $H\gamma$ feature to understand its power in breaking the well known degeneracy. In § 2 we use the high spectral resolution ($\text{FWHM} \sim 1.8\text{\AA}$) single-age, single-metallicity stellar populations (SSP’s) model library of Vazdekis (1999) (hereafter V99) and find that $H\gamma_{HR}$ is strongly dependent on resolution and galaxy velocity dispersion. In § 3 we study $H\gamma$ as a function of age, metallicity and resolution and define a new indicator which is completely insensitive to metallicity and stable against resolution. We deal with the most important problems affecting this indicator and propose a recipe for determining the average stellar age of a galaxy. In § 4 we present a discussion and in § 5 our conclusions.

2. The $H\gamma$ feature

2.1. The SSP spectral library

To study H γ feature we use the spectral synthesis model of V99 (an extended version of the evolutionary stellar population synthesis model of Vazdekis et al. 1996) which predicts spectral energy distributions (SED's) for single-aged old stellar populations with metallicities $-0.7 \leq [Fe/H] \leq +0.2$ at resolution FWHM $\sim 1.8\text{\AA}$ in the optical region. The model uses as input database the empirical spectral library of Jones (1997), after a careful selection of a subsample of ~ 550 stars. One important advantage of this model is that it allows direct measurements of particular absorption features on the spectra of SSP's with specified metallicity, age, and initial stellar mass function (IMF), instead of employing polynomial fitting functions that relate the absorption line-strengths with the stellar atmospheric parameters (Worthey 1994; Vazdekis et al. 1996). We use the *bimodal IMF* of Vazdekis et al. (1996) with a shallow low-mass ($\leq 0.6M_{\odot}$) slope and a Salpeter (1955) high mass slope.

2.2. The behavior of H γ as a function of resolution

In V99 we showed the intermediate resolution indices H γ_A and H γ_F (Worthey & Ottaviani 1997) and the high resolution index H γ_{HR} (JW95) as a function of the age and metallicity for SSP's. Unexpectedly, the two set of indices show opposite trends: at specified age, most metal-deficient SSP's give largest values for H γ_A and H γ_F but H γ_{HR} . Moreover, the wavelength baselines covered by H γ_A and H γ_F are considerably larger than the one by H γ_{HR} . This fact suggests that H γ is not only sensitive to resolution but also to the way in which the index is defined, as was pointed out by JW95. We therefore speculate that there must be a particular definition (with wavelength coverage larger than in H γ_{HR} but shorter than in H γ_F and H γ_A , where the index is insensitive to metallicity. Fig. 1 shows H γ_{HR} as a function of the metallicity and age of the SSP for different resolutions σ 's. For $\sigma = 60 \text{ kms}^{-1}$ the most metal-rich SSP's provide the largest values. This tendency is much less pronounced for $\sigma = 125 \text{ kms}^{-1}$, where the previous trend is starting to change (e.g., the values for $[Fe/H]=-0.4$ are larger than those for $[Fe/H]=0.0$). For $\sigma = 200 \text{ kms}^{-1}$ we get the maximum convergence of the lines; this resolution seems to be the *inflection point* at which all loci with different metallicities converge. Finally, for $\sigma = 275 \text{ kms}^{-1}$ the trend is completely inverted (resembling H γ_A and H γ_F).

Fig. 2 shows various SSP model spectra of 13 Gyr and different metallicities broadened to the resolutions used in Fig. 1. In first panel we mark the definition of H γ_{HR} , which measures the EW of a total area of 3.74\AA centered on H γ by selecting as pseudocontinua the left and right peaks (indicated by arrows).

While $H\gamma$ has nearly the same depth, the metallic contribution from its left side is strengthening the feature for more metal-rich populations. For stars, the dependence of $H\gamma_A$, $H\gamma_F$, and $H\gamma_{HR}$ as a function of T_{eff} was shown by Worthey & Ottaviani (1997) and Jones (1997) respectively: in all cases the EW increases very sharply for T_{eff} 's larger than ~ 5500 K, but for lower T_{eff} 's where $H\gamma$ is basically constant. Since old stellar populations have T_{eff} 's in this lower temperature range, differences in T_{eff} due to changes in metallicity are not enough to vary the absorption strength rapidly enough to compensate the very slow change of $H\gamma$. We conclude that for old stellar populations the strengthening of $H\gamma_{HR}$ as a function of metallicity is mainly caused by its adjacent blue side metallic absorption. When broadening the spectra to $\sigma = 125 \text{ km s}^{-1}$ these metallic features are merged with $H\gamma$ line. However the adopted pseudocontinua start to be depressed by the deepening of the strong neighboring FeI lines centered on 4325 \AA and 4352 \AA (the latter also contains MgI), affecting $H\gamma_{HR}$ strength in the reverse sense. For $\sigma = 200 \text{ km s}^{-1}$ these pseudocontinua are more depressed (than for $\sigma = 125 \text{ km s}^{-1}$) for more metal-rich SSP's, making $H\gamma_{HR}$ nearly identical. This is what we have called the inflection point, where metallicity effects are negligible. Finally, for $\sigma = 275 \text{ km s}^{-1}$ the pseudocontinua are considerably depressed, breaking the effect that occurs at 200 km s^{-1} , and causing larger EW's for most metal-deficient SSP's. Unfortunately, due to limitations in model parameter coverage, we are unable to study in detail the inflection point for SSP's of younger ages and/or lower metallicities.

3. The new age indicator

3.1. New index definitions

Fig. 1 shows that $H\gamma_{HR}$ provides a stronger power at separating age at $\sigma = 200 \text{ km s}^{-1}$ than for lower or higher resolutions. JW95 calculated $H\gamma_{HR}$ for SSP's using a different approach: they derived empirical fitting functions which relate the stellar atmospheric parameters to the measured line-strengths on the basis of Jones (1997) stellar library (after broadening the spectra to $\sigma = 83 \text{ km s}^{-1}$). Their $H\gamma_{HR}$ model predictions fall among the first two plots of Fig. 1 (i.e. those calculated for $\sigma = 60$ and 125 km s^{-1}). Fig. 1 also shows that $H\gamma_{HR}$ is very sensitive to resolution due to the selection of these two peaks as pseudocontinua (which also vary in height and position as a function of metallicity). Thus, $H\gamma_{HR}$ age disentangling power is destroyed with very small σ changes.

To achieve a metallicity insensitive $H\gamma$ indicator which is stable against σ we used the following approach: first we broadened the SSP spectral library of V99 by steps of 25 km s^{-1} from $\sigma = 60 \text{ km s}^{-1}$ to $\sigma = 400 \text{ km s}^{-1}$. We propose various $H\gamma$ index definitions, and then we measure them on these model

spectra. We find new indices, $[\text{H}\gamma+1/2(\text{FeI}+\text{MgI})]_{\sigma}$, which are completely insensitive to metallicity, at well separated resolutions: $\sigma = 125 \text{ kms}^{-1}$, 200 kms^{-1} and 275 kms^{-1} , each quite stable in a range of $\Delta\sigma \sim 75 \text{ kms}^{-1}$. Table 1 provides the new definitions (also marked in Fig. 2).

$[\text{H}\gamma+1/2(\text{FeI}+\text{MgI})]_{125}$ uses the effect of the blue pseudocontinuum to precisely guarantee this ability to disentangle the age, while for the red pseudocontinuum it uses a portion of the very stable continuum around 4364\AA . To achieve the resolution stability (required for practical applications) we select the blue pseudocontinuum to fall into the bottom of $\text{H}\gamma$ ($\lambda=4340.468\text{\AA}$), and the feature to fall well inside this pseudocontinuum. This selection introduces a change that is cancelled by extending the red edge of our feature to the bottom of $\text{FeI}+\text{MgI}$ at $\lambda=4352.737\text{\AA}$ (FeI): for increasing metallicities the strength lost due to blue pseudocontinuum depression (caused by the strengthening of FeI at 4325\AA and by the full inclusion in this pseudocontinuum of $\text{H}\gamma$ blue side metallic absorption) is cancelled with the depth gained by $\text{FeI}+\text{MgI}$ strengthening (which is contributing to the feature in the new definition). Thus this index is not just an EW as we are dealing with the *absorption line profile*, and then it is required spectroscopy of very high signal-to-noise ratio and relatively high dispersion (see § 3.2). At this level of accuracy, an influence of the stellar kinematics cannot be neglected. In particular, kinematically complex systems (e.g., Prada et al. 1996) would require a simultaneous line profiles and kinematics processing.

Modifying these definitions slightly, we find similar age-metallicity trends for $\sigma = 200 \text{ kms}^{-1}$ and $\sigma = 275 \text{ kms}^{-1}$, providing equally stable σ ranges. These indices allow us to cover almost the whole range of galaxy σ 's up to $\sim 300 \text{ kms}^{-1}$. However, despite the fact that such inflection point can essentially be found for larger σ 's ($\sim 400 \text{ kms}^{-1}$), resulting solutions were not stable against resolution. Fig. 3 demonstrates the robustness and age disentangling power of $[\text{H}\gamma+1/2(\text{FeI}+\text{MgI})]_{\sigma}$ system. Bottom-left panel of Fig. 3 shows $[\text{H}\gamma+1/2(\text{FeI}+\text{MgI})]_{125}$ stability against resolution. Table 2 tabulates the mean index values for various ages of the SSP's. We also note that $[\text{H}\gamma+1/2(\text{FeI}+\text{MgI})]_{\sigma}$ indices are probably not unique for achieving this age discriminating power and alternative definitions could well be sought.

3.2. Index characteristics and major uncertainties

In this section we study the problems that can affect $[\text{H}\gamma+1/2(\text{FeI}+\text{MgI})]_{\sigma}$ indicators for practical applications. Table 3 summarizes their characteristics and major uncertainties.

3.2.1. Spectral resolution

The spectral resolution effect is extensively discussed in § 3.1. Table 3 tabulates σ ranges where $[\text{H}\gamma+1/2(\text{FeI}+\text{MgI})]_\sigma$ indices are stable against resolution. Within these ranges ($\Delta\sigma \sim 45 \text{ kms}^{-1}$) it is possible to distinguish models of 13 Gyr and 17 Gyr, irrespective of the metallicity (in the range $-0.7 \leq [\text{Fe}/\text{H}] \leq +0.2$). Bottom-left panel of Fig. 3 shows that $[\text{H}\gamma+1/2(\text{FeI}+\text{MgI})]_\sigma$ indices are also stable within $\Delta\sigma \sim 75 \text{ kms}^{-1}$ but the age disentangling power decreases slightly (only SSP’s younger than 12 Gyr can be distinguished from one of 17 Gyr).

3.2.2. Signal-to-noise ratio

Unfortunately, the required signal-to-noise ratio per \AA , $S/N(\text{\AA})$, is very high, limiting the number of galaxies observable with most of present-day intermediate class telescopes. An estimate of the required exposure time can be done using the analytical approach of Cardiel et al. (1998) (eqs. (9) and (41) to (44)). Following their notation, coefficients c_1 and c_2 are calculated from eqs. (43) and (44) using Table 1 index definitions. Assuming a desirable index error ($\sigma[I_a]$), we use eq. (41) to estimate the required $S/N(\text{\AA})$ (SN). Then by approaching $\sigma_i(\lambda_i) \sim \sqrt{S(\lambda_i)}$, we use eq. (42) to obtain the number of counts per ADU:

$$c = \frac{SN\theta}{2g} \left[SN + \sqrt{SN^2 + \frac{4\sigma_{RN}^2}{\theta}} \right], \quad (1)$$

where θ is the dispersion in \AA per resolution element, g is the gain in e^{-1}/ADU , σ_{RN} is the readout noise in e^{-1} . Finally we compare with the signal obtained in real observational runs. An example in which we integrate all photons within $\sim 2''$ for a nearby galaxy center with $\mu_B = 17.5 \text{ mag arcsec}^{-2}$ on a 4m class telescope is given in Table 3. We used $\theta = 0.8 \text{ \AA}/\text{pix}$ and $\sigma_{RN} = 4.4 e^{-1}$. Table 3 also shows that higher resolution $[\text{H}\gamma+1/2(\text{FeI}+\text{MgI})]_\sigma$ definitions require lower S/N ’s.

3.2.3. Wavelength and radial velocity uncertainties

Table 3 shows largest λ errors or shifts allowed to guarantee $[\text{H}\gamma+1/2(\text{FeI}+\text{MgI})]_\sigma$ age disentangling power. Thus irrespective of galaxy σ ’s, observational spectra of relatively high dispersion ($\lesssim 0.8 \text{\AA}$) are required to achieve an accurate λ calibration that is typically $\sim 5\text{-}10\%$ of the adopted dispersion. This also implies that radial velocity effects such as galaxy internal rotational velocity or redshift should be taken into account with high precision. For this purpose the observed spectrum should be crosscorrelated with

an appropriate V99 model spectrum (see Appendix). We also note that a galaxy with a recession velocity of $\sim 1000 \text{ km s}^{-1}$ produces a difference of $\sim 0.13 \text{ \AA}$ between the bluest point of the blue pseudocontinuum and the reddest point of the red pseudocontinuum, i.e., as large as the largest λ shift allowed for $[\text{H}\gamma+1/2(\text{FeI}+\text{MgI})]_{125}$. Therefore the $(1+z)$ effect should be properly accounted for.

3.2.4. *The spectrum shape*

The effect of the spectrum shape on $[\text{H}\gamma+1/2(\text{FeI}+\text{MgI})]_{\sigma}$ should be small because the wavelength range involved is quite narrow. We have done the following test: we removed the continuum of V99 model spectra (using an spline3 of order 6) and then measured $[\text{H}\gamma+1/2(\text{FeI}+\text{MgI})]_{\sigma}$. Table 3 shows the largest differences (obtained for the oldest SSP’s) when comparing to previous measurements (i.e., on the SSP spectra with a flux calibrated response). We conclude that the effect of the instrumental response curve on $[\text{H}\gamma+1/2(\text{FeI}+\text{MgI})]_{\sigma}$ is nearly negligible.

3.2.5. *Age uncertainties*

Table 3 summarizes the largest theoretical age uncertainties as well as the ones obtained when adopting the largest errors allowed either in σ , $\Delta\lambda$ (e.g., errors in λ calibration, redshift, rotation curve) or S/N slightly lower than recommended.

3.3. **A recipe for determining the luminosity-weighted average stellar age of a galaxy**

A detailed description of the main characteristics and uncertainties of $[\text{H}\gamma+1/2(\text{FeI}+\text{MgI})]_{\sigma}$ indices was performed in § 3.2. Here we summarize the steps required to ensure a correct index measurement:

1. The observed spectrum should satisfy the high S/N requirement of Table 3, which can be achieved by integrating over the spatial direction. Dispersion should be large enough (preferably $< 0.8 \text{ \AA}/\text{pix}$) to prevent absolute $\Delta\lambda$ shifts or errors with a precision as given in Table 3.
2. Determine σ along the spatial direction (e.g., by using stellar template spectra acquired with the same instrumental configuration, or by using V99 models). Very accurate σ measurement is not essential.

3. Crosscorrelate the observed spectrum with an appropriate V99 model spectrum (instead of using a stellar template) to determine its absolute radial velocity, which has to be taken into account when measuring the index (see Appendix). This is a very important step.
4. Integrate over spatial direction to achieve the required S/N. Variations of velocity rotation (and σ) must be smaller than indicated in Table 3. Otherwise they should be carefully taken into account.
5. Measure $[\text{H}\gamma+1/2(\text{FeI}+\text{MgI})]_{\sigma}$ index appropriate for obtained σ and compare with Table 2 to estimate the age¹. A fortran code is provided at our web site: <http://www.ioa.s.u-tokyo.ac.jp/~vazdekis/>.

4. Discussion

First panel of Fig. 3 shows $[\text{H}\gamma+1/2(\text{FeI}+\text{MgI})]_{125}$ measurements for two metal-rich globular clusters of our Galaxy, 47 Tuc and NGC 6624 (Rose 1994), five low velocity dispersion ellipticals of Jones (1997) (NGC 4489, NGC 4239, NGC 3605, NGC 4387 and M 32) and the standard S0 galaxy NGC 7332 (Vazdekis 1996). The latter spectrum, with 1 *hour* exposure time, was obtained at Observatorio del Roque de Los Muchachos, La Palma, using the 4.2m WHT (ISIS spectrograph). We integrate the innermost 1.5'' along the slit (positioned on the minor axis of the galaxy) to achieve a relatively high (although not enough) $\text{S/N}(\text{\AA})\sim 140$. Rotation curve and σ were both found to be very stable in this region. All these spectra (except NGC 7332 which has $\sigma \sim 135 \text{ kms}^{-1}$) were pre-broadened to a common resolution of 125 kms^{-1} .

The M 32 spectrum (with extremely high S/N, see JW95) was broadened to $\sigma = 200 \text{ kms}^{-1}$ and 275 kms^{-1} for measuring $[\text{H}\gamma+1/2(\text{FeI}+\text{MgI})]_{200}$ and $[\text{H}\gamma+1/2(\text{FeI}+\text{MgI})]_{275}$ respectively (see right panels of Fig. 3). Obtained ages (using Table 2) are in good internal consistency since the three indices provide ~ 4 Gyr. JW95 obtained ~ 7 Gyr on the basis of $\text{H}\gamma_{HR}$. This difference could be attributed in part to the fact that the stellar isochrones adopted in Worthey's (1994) population synthesis model are systematically hotter than those used in Vazdekis et al. (1996), and to possible effects caused by the fact that $\text{H}\gamma_{HR}$ is strongly sensitive to very small σ variations. However our age estimation is in full agreement with an extraordinary fit that we have obtained for this galaxy using V99 models (see Fig. 4 and Appendix).

¹If obtained σ falls outside $[\text{H}\gamma+1/2(\text{FeI}+\text{MgI})]_{\sigma}$ resolution stability range (see Table 3), results improve slightly if the observational spectrum is broadened (by convolving with a gaussian) to match σ of the index. However the reader should be aware that higher resolution definitions require lower S/N's (see Table 3).

The two clusters are found to be very old ($\gtrsim 13$ Gyr). This sample of low-luminosity ellipticals show a rather large spread in age; NGC 4489 (~ 3 Gyr), M 32 (~ 4 Gyr), NGC 4239 (~ 5.5 Gyr), NGC 3605 (~ 7.5 Gyr) and NGC 4387 (~ 12 Gyr), respectively. Finally, for NGC 7332 we obtain ~ 6 Gyr (in full agreement with Vazdekis 1996). Since our results are based on SSP model predictions this method estimates luminosity-weighted average stellar ages, but cannot tell whether this spread is due to a real difference of *mean stellar age*, implying different epoch of galaxy formation, or caused by a contamination of intermediate age stars formed in a secondary episode of star formation (Kodama & Arimoto 1998).

$[\text{H}\gamma+1/2(\text{FeI}+\text{MgI})]_{\sigma}$ indices cover most of galaxy σ 's range (up to 300 km^{-1}). In this paper we derive average ages for globular clusters and low-luminosity ellipticals. However we stress that these indices are fully applicable to normal and giant ellipticals, including cD's. Once high S/N spectra of relatively high dispersion are obtained, accurate and reliable estimates for the average stellar ages of these galaxies will be possible, without assessing their metallicities. Once the age is determined, metallicity can be evaluated uniquely from key metallic lines. The age-metallicity degeneracy of line indices is solved. We note that $[\text{H}\gamma+1/2(\text{FeI}+\text{MgI})]_{\sigma}$ indices are probably not unique as age indicators for old stellar populations. Other Balmer lines with neighboring metallic lines could also produce a similar effect and need to be addressed.

Direct estimates of galaxy age would provide a definitive answer to the origin of the CMR which is tightly followed by cluster elliptical galaxies (e.g., Bower, Lucey & Ellis 1992). Field ellipticals and small groups of galaxies might have formed differently from those in rich clusters. González (1993) showed that field ellipticals have significantly stronger H_{β} indices than expected from Worthey's (1994) models of very old age. This implies that they could be younger than cluster ellipticals. However H_{β} is not an accurate age indicator since its dependence on metallicity is not negligible, and since it could be easily filled in with nebular emission (Davies et al. 1993) even for early-type galaxies. $\text{H}\gamma$ is substantially less affected.

It is well known that stars in the Galactic halo, including those in globular clusters, are enhanced in α -elements (e.g., Mg, Si, Ca) with respect to Fe (Edvardsson et al. 1993). Giant elliptical galaxies show $[\alpha/\text{Fe}] \simeq +0.3$ (Peletier 1989, Worthey, Faber & González 1992, Vazdekis et al. 1997). This may cause a small effect on the resulting age estimate, because we have assumed solar abundance ratios throughout the present study (although $[\text{H}\gamma+1/2(\text{FeI}+\text{MgI})]_{\sigma}$ includes both Fe and Mg in its definition). Worthey (1998) suggested that abundance ratio changes can cause changes in isochrone temperature structure that can mimic an age effect. Salaris & Weiss (1998) have shown that scaled-solar isochrones no longer can be used to replace α -enhanced ones at the same total metallicity. Unfortunately, empirical spectra of stars with

different $[\alpha/Fe]$ ratios are not yet available and we cannot assess this problem for the moment.

5. Conclusions

We define new spectral indices, $[H\gamma+1/2(FeI+MgI)]_\sigma$, which are robust age indicators for old and relatively old stellar populations and therefore have a great potential for breaking the age-metallicity degeneracy of galaxy spectra. To achieve this we use the new evolutionary stellar population synthesis model of Vazdekis (1999) which provides SED's of SSP's at $FWHM \sim 1.8\text{\AA}$. These new models not only allow us to investigate the behavior of $H\gamma$ as a function of metallicity and age, but also as a function of spectral resolution by performing a direct measurement of the feature on the synthesized SSP spectra broadened to different σ 's. We show that the strong power of $H\gamma$ to disentangle the age is due to a compensating effect: at specified age the strengthening of $H\gamma$ is mainly caused by its adjacent metallic absorption which is more prominent for more metal-rich populations. On the other hand the adopted pseudocontinua are depressed by the effects of the strong neighboring FeI lines on both sides of $H\gamma$ (centered on 4325\AA and 4352\AA). On the basis of this effect we achieve new $H\gamma$ index definitions that are completely insensitive to the metallicity in the range $-0.7 \leq [Fe/H] \leq +0.2$. However, since this effect is strongly dependent on the adopted resolution and galaxy velocity dispersion, we have optimized $H\gamma$ definitions for assessing the resolution stability required for practical applications. We propose unprecedented age indicators, $[H\gamma+1/2(FeI+MgI)]_\sigma$, at well separated velocity dispersions: $\sigma = 125, 200, \text{ and } 275 \text{ kms}^{-1}$, and each is stable in a range of $\Delta\sigma \sim 75 \text{ kms}^{-1}$, thus allowing study of most galaxies up to $\sigma \sim 300 \text{ kms}^{-1}$.

The main characteristics and uncertainties affecting $[H\gamma+1/2(FeI+MgI)]_\sigma$ are extensively discussed. Since we are dealing with the absorption profile of $H\gamma$, observational spectra of very high signal-to-noise ($S/N(\text{\AA}) \gtrsim 200$) and relatively high dispersion ($\lesssim 0.8\text{\AA}/\text{pix}$), but feasible for luminous nearby galaxies with 4m class telescopes, are required to gain this unprecedented age discriminating power. We provide a recipe for a correct measurement of $[H\gamma+1/2(FeI+MgI)]_\sigma$: determine σ of the observed spectrum, determine its absolute radial velocity (by using a synthetic spectrum which match best the age/metallicity of the galaxy), measure the index appropriate for that velocity dispersion, and compare with the metallicity-insensitive model values of Table 2 to estimate the age. High S/N's can be achieved by integrating along the spatial direction if variations of velocity rotation (and σ) are properly accounted for.

Once observational spectra of high quality are acquired, accurate and reliable estimates for the luminosity-weighted average stellar ages of these galaxies will be possible for the first time, without assessing

their metallicities. In this paper we perform such measurements for two metal-rich globular clusters, a sample of low-luminosity ellipticals and a standard S0 galaxy. We find a large spread in the average stellar ages of these low-luminosity ellipticals. In particular, these indices yield 4 Gyr for M 32. This value is in excellent agreement with the age provided by an extraordinary fit to the full spectrum of this galaxy that we achieve in this paper.

We are indebted to J. Rose and L. Jones for providing their globular cluster and elliptical galaxy spectra. We are grateful to V. Vanevičius and R. Peletier for very interesting comments and suggestions. We are also grateful to the referee for useful corrections and suggestions. A.V. thanks the Japan Society for Promotion of Science for financial support. This work was financially supported in part by a Grant-in-Aid for the Scientific Research (No.09640311) by the Japan Ministry of Education, Culture, Sports and Science.

A. Accurate absolute radial velocity determination for measuring $[\text{H}\gamma+1/2(\text{FeI}+\text{MgI})]_{\sigma}$

Accurate radial velocity determinations can be achieved if an observational galaxy spectrum is crosscorrelated with a template which resembles best the galaxy (e.g. Tonry & Davis 1979). This approach would benefit substantially if templates are chosen from the new SSP model spectral library of V99, rather than using observations of a template star (which could easily be a poor match, thus producing a crosscorrelation peak with asymmetrical wings that could bias the centroid of the fitting function, e.g., gaussian). Therefore we strongly suggest the use as templates of at least various synthetic spectra (FWHM \sim 1.8Å) of different ages (e.g., 1.5, 3, 6 and 12 Gyr) and metallicities ($[\text{Fe}/\text{H}]$ =-0.7, -0.4, 0.0, +0.2) which can be retrieved from our web site (<http://www.ioa.s.u-tokyo.ac.jp/~vazdekis/>). Choosing the model spectrum which provides the largest crosscorrelation peak height (i.e., produced by the most appropriate template), we determine accurately the absolute radial velocity and prevent any additional shifts to the models. Prior to crosscorrelation all the spectra should be rebinned logarithmically (with same dispersion), continuum removed (e.g., using a spline3 of low order). Results improve if the spectra are adequately filtered to remove their very high and very low frequencies, and multiplied by a cosine-bell-like function. Detailed explanations can be found in V99 (and references therein).

As an example, we have crosscorrelated M 32 spectrum (Jones 1997) with the whole SSP model spectral library of V99. Fig. 4 shows that the largest crosscorrelation peak height is obtained for a model of \sim 4 Gyr and $[\text{Fe}/\text{H}]$ =0.0. This implies that the use of this spectrum (or a similar one) as template would increase

the accuracy of the kinematical parameter determination. This model is overplotted on M 32 spectrum providing an extraordinary fit (see Fig. 4) which confirms the age predicted by $[\text{H}\gamma+1/2(\text{FeI}+\text{MgI})]_{\sigma}$.

REFERENCES

- Arimoto, N., 1996, ASP Conference Series, Vol. 98, *From Stars To Galaxies*, eds. C. Leitherer, U. Fritze-von Alvensleben & J. Huchra, p. 287
- Arimoto, N., & Yoshii, Y., 1987, *A&A*, 173, 23
- Bower, R.G., Lucey, J.R., Ellis, R.S., *MNRAS*, 254, 589
- Cardiel, N., Gorgas, J., Cenarro, J., González, J.J, 1998, *A&AS*, 127, 597
- Davies, R.L., Sadler, E.M., Peletier, R.F. 1993, *MNRAS*, 262, 650
- Edvardsson, B., Andersen, J., Gufstafsson, B., Lambert, D.L., Nissen, P.E., Tomkin, J., 1993, *A&A*, 275, 101
- Ferreras, I., Charlot, S. & Silk, J. 1998, *ApJ*, in press
- González, J.J, 1993, Ph.D. Thesis, Univ. of Lick, Santa Cruz, California
- Jones, L.A, 1997, Ph.D. Thesis, Univ. of North Carolina, Chapel Hill
- Jones, L. & Worthey, G., 1995, *ApJ*, 446, L31 (**JW95**)
- Kodama, T. & Arimoto, Y., 1997, *A&A*, 320, 41
- Kodama, T. & Arimoto, Y., 1998, *MNRAS*, 300, 193
- O’Connell, R., 1976, *ApJ*, 206, 370
- O’Connell, R., 1986, in *Stellar Populations*, ed. C. Norman, A. Renzini and M. Tosi, Cambridge University Press, p. 167
- Peletier, R.F., 1989, Ph. D. Thesis, Univ. of Groningen
- Prada, F., Gutiérrez, C.M., Peletier, R.F., McKeith, C.D. 1996, *ApJ*, 463, L9
- Rose, J.A., 1994, *AJ*, 107, 206
- Salaris, M., Weiss, A., 1998, *A&A*, 335, 943
- Salpeter, E., 1955, *ApJ*, 121, 161
- Tonry, J. & Davis, M. 1979, *AJ*, 84, 1511
- Vazdekis, A., 1999, *ApJ*, 513, 224 (**V99**)
- Vazdekis, A., 1996, Ph.D. Thesis, Univ. of La Laguna, Spain

Vazdekis, A., Peletier, R. F., Beckman, J. E. & Casuso, E., 1997, ApJS, 111, 203

Vazdekis, A., Casuso, E., Peletier, R. F. & Beckman, J. E., 1996, ApJS, 106, 307

Worthey, G., 1998, PASP, 110, 888

Worthey, G., 1994, ApJS, 95, 107

Worthey, G. & Ottaviani, D.L., 1997, ApJS, 111, 377

Worthey, G., Faber, S., González, J., 1992, ApJ, 398, 69 ApJS, 94, 687

Fig. 1.— $H\gamma_{HR}$ index measured on V99 model spectral library broadened to various resolutions: $\sigma = 60 \text{ kms}^{-1}$, 125 kms^{-1} , 200 kms^{-1} , and 275 kms^{-1}

Fig. 2.— Model spectra of 13 Gyr and $[\text{Fe}/\text{H}] = -0.7$ (dot-dashed lines), $[\text{Fe}/\text{H}] = -0.4$ (dotted lines), $[\text{Fe}/\text{H}] = 0.0$ (solid lines) and $[\text{Fe}/\text{H}] = +0.2$ (dashed lines), broadened to the resolutions used in Fig 1. All these spectra were normalized to 1 at 4365\AA . On the first panel we mark $H\gamma_{HR}$ definition of JW95 (the arrows indicate the positions of the adopted continua), while on the other panels we mark $[\text{H}\gamma+1/2(\text{FeI}+\text{MgI})]_{\sigma}$ definition for each resolution: thick dotted lines represent the feature while thick solid lines represent the pseudocontinua

Fig. 3.— $[\text{H}\gamma+1/2(\text{FeI}+\text{MgI})]_{\sigma}$ indices measured on the same SSP's spectra of Fig. 1. On the first panel, open stars represent $[\text{H}\gamma+1/2(\text{FeI}+\text{MgI})]_{125}$ values measured on the spectra of two metal-rich globular clusters (47 Tuc and NGC 6624). Open circles are the values obtained for a sample of low-luminosity ellipticals of Jones (1997). Open polygon represents the value for the central region of the NGC 7332 S0 galaxy (Vazdekis 1996). The largest error bar is also plotted. Table 2 was used to infer the age. M 32 spectrum was broadened to $\sigma \sim 200 \text{ kms}^{-1}$ and $\sim 275 \text{ kms}^{-1}$ for measuring $[\text{H}\gamma+1/2(\text{FeI}+\text{MgI})]_{200}$ (upper-right panel) and $[\text{H}\gamma+1/2(\text{FeI}+\text{MgI})]_{275}$ (bottom-right panel) respectively, providing the same age (4 Gyr). Finally, the bottom-left panel represents a test to the stability of $[\text{H}\gamma+1/2(\text{FeI}+\text{MgI})]_{125}$; measured on the model spectra after broadening to $\sigma = 100 \text{ kms}^{-1}$ (thin lines for different metallicities), $\sigma = 125 \text{ kms}^{-1}$ (thick lines, i.e. the same values as in the upper-left panel) and $\sigma = 175 \text{ kms}^{-1}$ (very thick lines)

Fig. 4.— Upper panel shows the crosscorrelation peak height of M 32 spectrum with V99 model spectral library. All these spectra were broadened to $\sigma = 125 \text{ kms}^{-1}$. Lower panel shows M 32 spectrum and the synthetic spectrum which provided the largest crosscorrelation peak height, achieving an extraordinary fit

Index	Blue pseudocont.		Feature		Red pseudocont.	
$[H\gamma+1/2(\text{FeI}+\text{MgI})]_{125}$	4330.000	4340.468	4333.000	4352.737	4359.250	4368.750
$[H\gamma+1/2(\text{FeI}+\text{MgI})]_{200}$	4331.000	4340.750	4332.000	4352.250	4359.250	4368.750
$[H\gamma+1/2(\text{FeI}+\text{MgI})]_{275}$	4331.500	4341.000	4331.500	4351.875	4359.250	4368.750

Table 1: $[H\gamma+1/2(\text{FeI}+\text{MgI})]_{\sigma}$ index definitions

Age	$[\text{H}\gamma+1/2(\text{FeI}+\text{MgI})]_{125}$	$[\text{H}\gamma+1/2(\text{FeI}+\text{MgI})]_{200}$	$[\text{H}\gamma+1/2(\text{FeI}+\text{MgI})]_{275}$
1.6	1.366	0.824	0.534
2.0	1.289	0.773	0.498
2.5	1.186	0.702	0.446
3.0	1.140	0.672	0.425
4.0	1.062	0.619	0.387
5.0	1.021	0.592	0.368
6.0	0.997	0.575	0.357
7.0	0.965	0.553	0.342
8.0	0.929	0.530	0.325
9.0	0.908	0.516	0.316
10.0	0.887	0.502	0.306
11.0	0.869	0.492	0.299
12.0	0.851	0.480	0.291
13.0	0.843	0.476	0.288
14.0	0.833	0.469	0.283
15.0	0.828	0.466	0.280
16.0	0.820	0.461	0.278
17.0	0.812	0.457	0.274
17.4	0.809	0.455	0.273

Table 2: Predicted index values for different ages. The tabulated numbers are obtained by averaging the index values obtained for different metallicities. The σ ranges in which these indices are very stable against resolution are: $115 - 160 \text{ kms}^{-1}$ for $[\text{H}\gamma+1/2(\text{FeI}+\text{MgI})]_{125}$, $165 - 210 \text{ kms}^{-1}$ for $[\text{H}\gamma+1/2(\text{FeI}+\text{MgI})]_{200}$ and $240 - 285 \text{ kms}^{-1}$ for $[\text{H}\gamma+1/2(\text{FeI}+\text{MgI})]_{275}$

	$[\text{H}\gamma+1/2(\text{FeI}+\text{MgI})]_{125}$	$[\text{H}\gamma+1/2(\text{FeI}+\text{MgI})]_{200}$	$[\text{H}\gamma+1/2(\text{FeI}+\text{MgI})]_{275}$
Optimal spectral resolution $\sigma(\text{kms}^{-1})$	125	200	275
Stability $\sigma(\text{kms}^{-1})$ range	100-175	150-225	225-300
Recommended $\sigma(\text{kms}^{-1})$ range	115-160	165-210	240-285
Required S/N per \AA	~ 200	~ 300	~ 400
Exp.time($\mu_B=17.5, \text{Int.}=2'', \text{Tel.}=4.2\text{m}, 0.8\text{\AA}/\text{pix}, \sigma_{RN}=4.4$)	~ 1.5 hour	~ 3 hour	~ 5 hour
Maximum $\Delta\lambda$ shift (e.g., errors in λ , z , rot. curve)	0.12\AA	0.08\AA	0.07\AA
$\Delta[\text{H}\gamma+1/2(\text{FeI}+\text{MgI})]_{\sigma}$ (Flux calib. - Continuum remov.)	$<0.022\text{\AA}$	$<0.015\text{\AA}$	$<0.009\text{\AA}$
Largest theoretical age uncertainty	14-17.5Gyr	14-17.5Gyr	14-17.5Gyr
Index error causing an age uncertainty of 11.5-17.5Gyr	$\sim 0.030\text{\AA}$	$\sim 0.021\text{\AA}$	$\sim 0.017\text{\AA}$

Table 3: Index characteristics and uncertainties

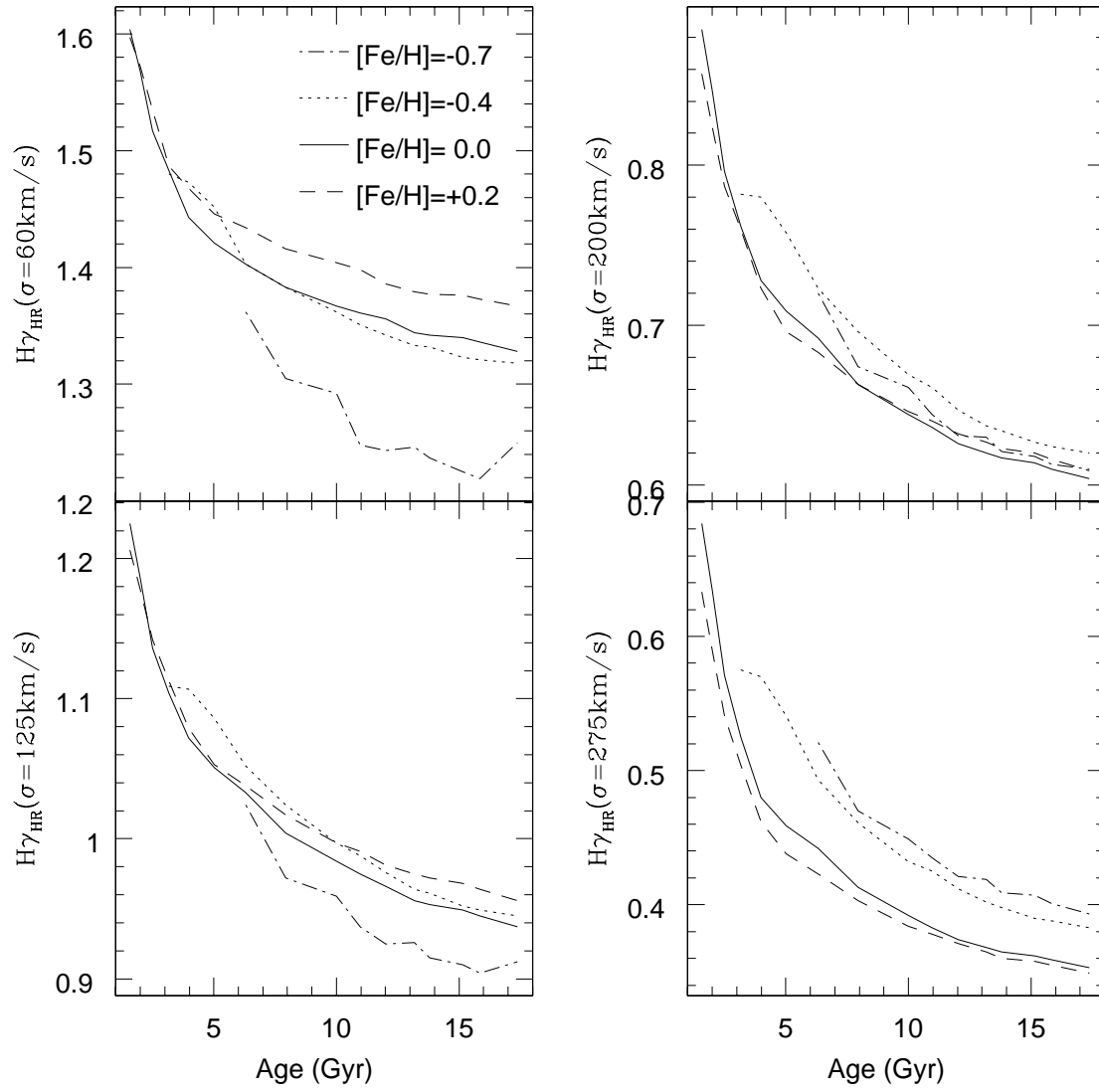


Fig. 1.—

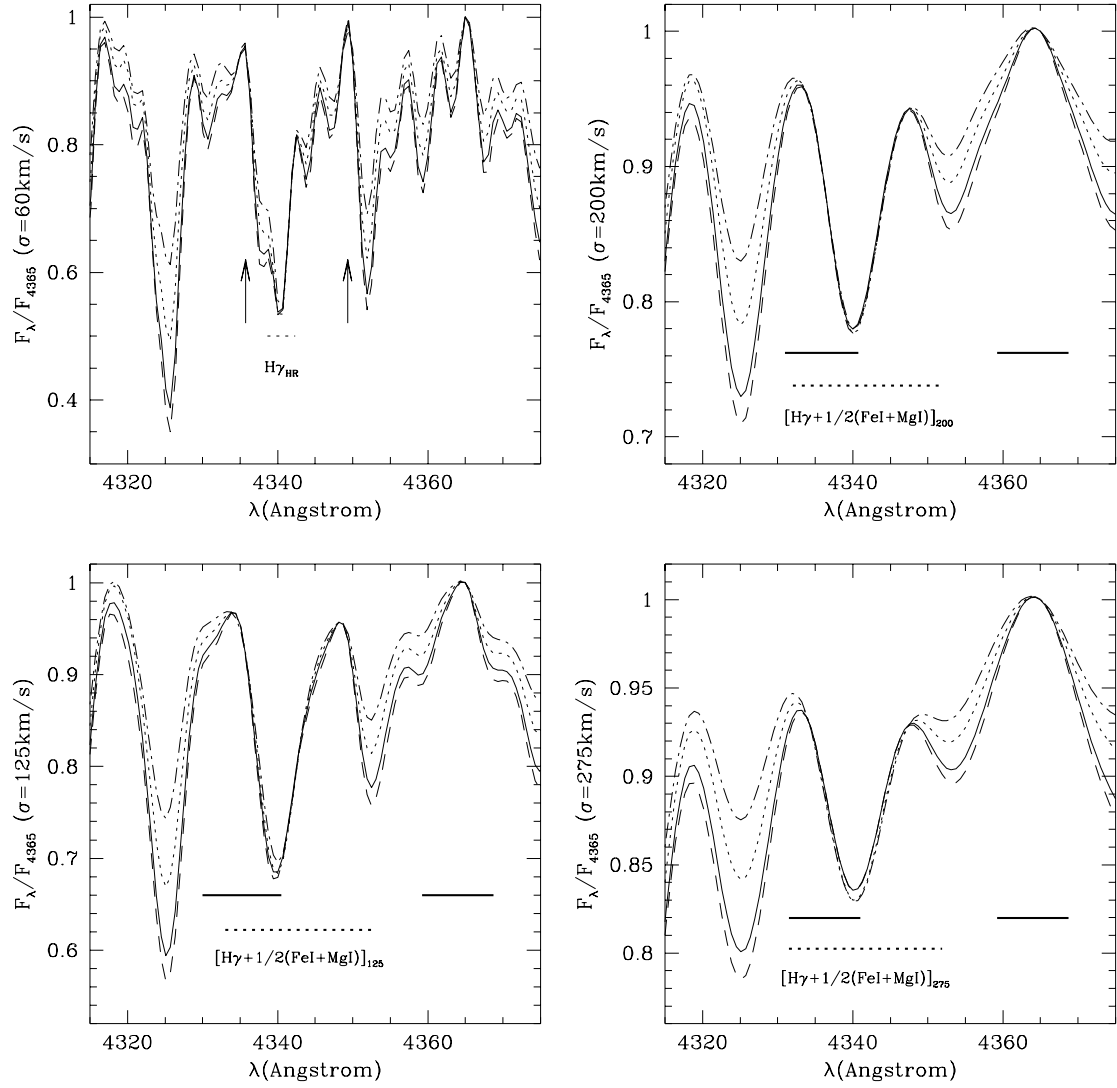


Fig. 2.—

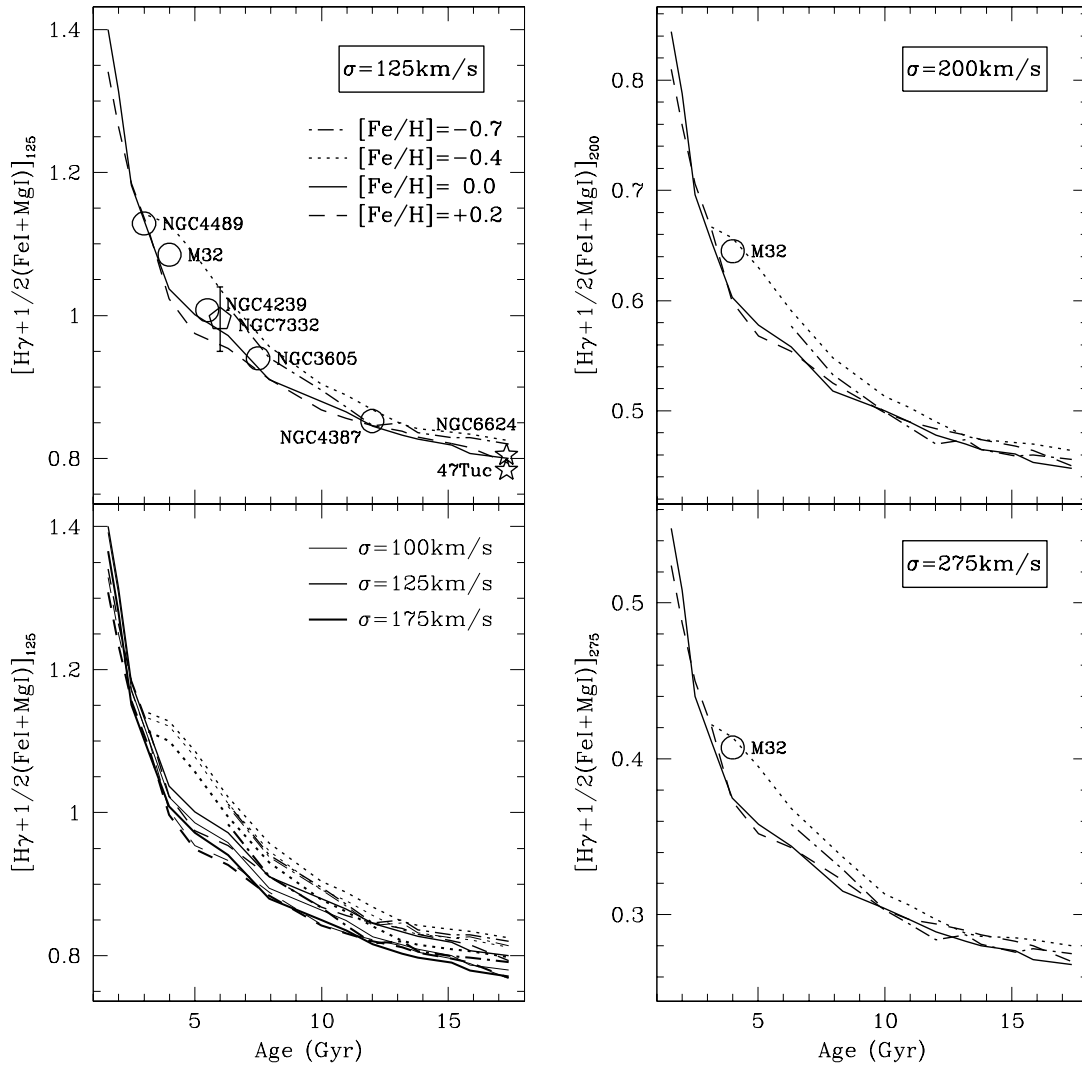


Fig. 3.—

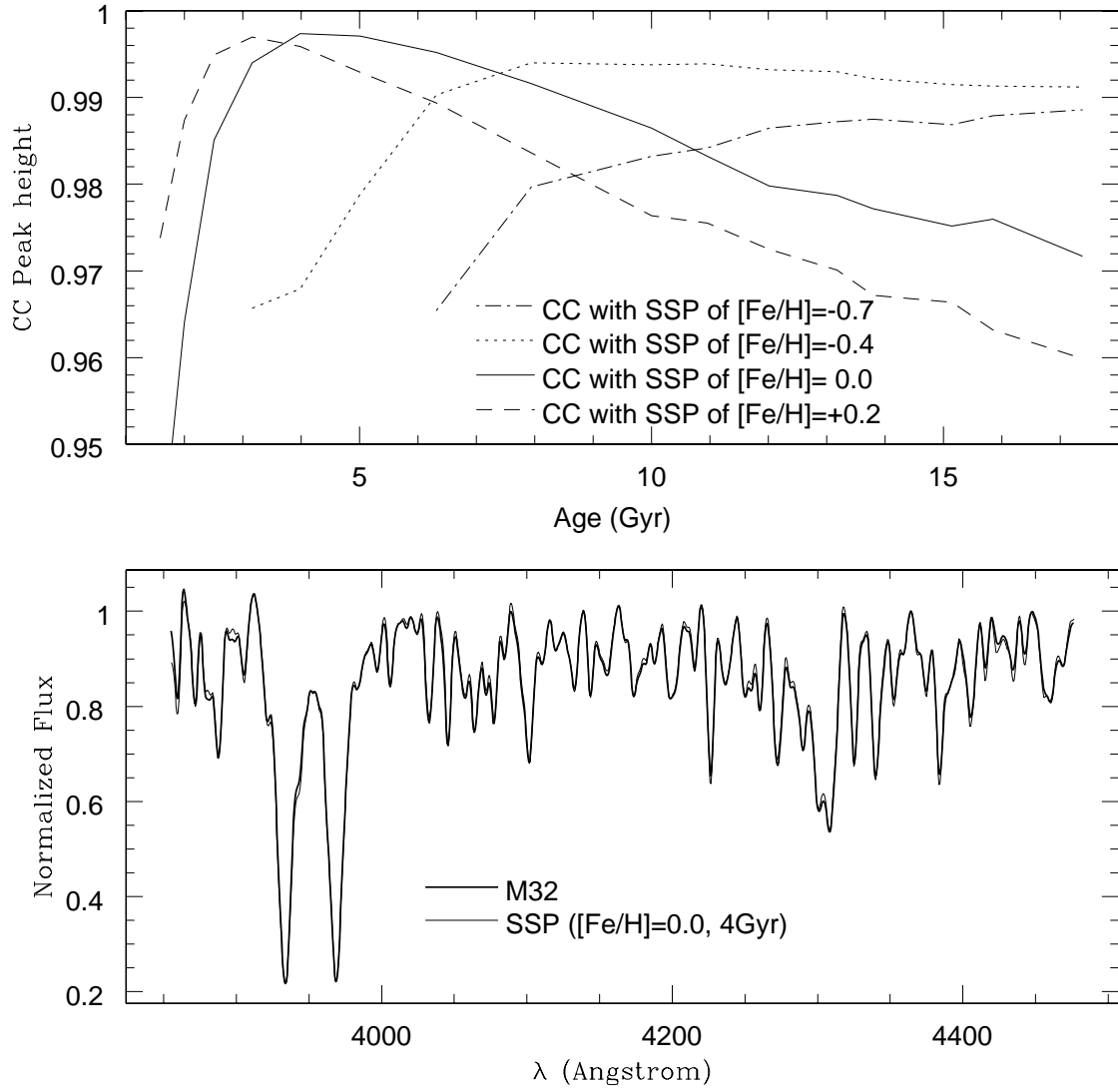


Fig. 4.—